# Photocrosslinkable Col/PCL/Mg composite membrane providing spatiotemporal maintenance and positive osteogenetic effects during guided bone regeneration

Feilong Wang [a,b,1], Dandan Xia [b,c,1], Siyi Wang [a,b], Ranli Gu [a,b], Fan Yang [a,b], Xiao Zhao [a,b], Xuenan Liu [a,b], Yuan Zhu [a,b], Hao Liu [b,d], Yongxiang Xu [b,c,**], Yunsong Liu [a,b,*], Yongsheng Zhou [a,b]

[a] Department of Prosthodontics, Peking University School and Hospital of Stomatology, Beijing, 100081, China
[b] National Engineering Laboratory for Digital and Material Technology of Stomatology, National Clinical Research Center for Oral Diseases, National Center of Stomatology, Beijing Key Laboratory of Digital Stomatology, Research Center of Engineering and Technology for Computerized Dentistry Ministry of Health, NMPA Key Laboratory for Dental Materials, Beijing, 100081, China
[c] Department of Dental Materials, Peking University School and Hospital of Stomatology, Beijing, 100081, China
[d] Central Laboratory, Peking University School and Hospital of Stomatology, Beijing, 100081, China

## ABSTRACT

Guided bone regeneration membranes have been effectively applied in oral implantology to repair bone defects. However, typical resorbable membranes composed of collagen (Col) have insufficient mechanical properties and high degradation rate, while non-resorbable membranes need secondary surgery. Herein, we designed a photocrosslinkable collagen/polycaprolactone methacryloyl/magnesium (Col/PCLMA/Mg) composite membrane that provided spatiotemporal support effect after photocrosslinking. Magnesium particles were added to the PCLMA solution and Col/PCLMA and Col/PCLMA/Mg membranes were developed; Col membranes and PCL membranes were used as controls. After photocrosslinking, an interpenetrating polymer network was observed by scanning electron microscopy (SEM) in Col/PCL and Col/PCL/Mg membranes. The elastic modulus, swelling behavior, cytotoxicity, cell attachment, and cell proliferation of the membranes were evaluated. Degradation behavior *in vivo* and *in vitro* was monitored according to mass change and by SEM. The membranes were implanted into calvarial bone defects of rats for 8 weeks. The Col/PCL and Col/PCL/Mg membranes displayed much higher elastic modulus ($p < 0.05$), and a lower swelling rate ($p < 0.05$), than Col membranes, and there were no differences in cell biocompatibility among groups ($p > 0.05$). The Col/PCL and Col/PCL/Mg membranes had lower degradation rates than the Col membranes, both *in vivo* and *in vitro* ($p < 0.05$). The Col/PCL/Mg groups showed enhanced osteogenic capability compared with the Col groups at week 8 ($p < 0.05$). The Col/PCL/Mg composite membrane represents a new strategy to display space maintenance and enhance osteogenic potential, which meets clinical needs.

## 1. Introduction

Bone defects affects the implantation success and long-term clinical efficacy of dental implants [1]. Guided bone regeneration (GBR) is the most common and well-documented strategy for horizontal and vertical alveolar bone defect augmentation [2,3] and has achieved positive outcomes [4,5]. The GBR membranes, also named barrier membranes [6], play a crucial role in preventing connective tissue and epithelium

migration to the defect, and reserving space for bone regeneration in the implantation site [7–9].

The ideal GBR membrane should have the following characteristics [6,10–12]: biocompatibility, occlusive properties, space maintenance capacity, the ability to attach to surrounding tissues, and clinical manageability. A wide variety of materials, such as collagen (Col) [13], polytetrafluorethylene [14], titanium [15], chitosan [16], polylactic acid (PLA), and polycaprolactone (PCL) [17], have been used as GBR membranes. These membranes can be categorized into two groups: resorbable and non-resorbable [5,6]. However, none of these membranes meet all of the required criteria. Most resorbable membranes are made of Col, and there are a variety of commercially available membranes [18]. Collagen membranes show excellent biocompatibility and can enhance osteoblast adhesion [6,12]. However, Col membranes lack space maintenance capacity and degrade too rapidly [19]; they only maintain barrier integrity for about 30 days [20,21]. Non-resorbable membranes have space maintenance capacity and occlusive properties, but always need a second surgery for removal, which increases the risk of infection and patient suffering [22]. Thus, it is necessary to develop new functional GBR membrane.

Polycaprolactone has been used in tissue-engineering scaffolds to regenerate bone, skin, and vascular tissues because of its superior toughness, mechanical strength, and biocompatibility [23–25]. It is a semicrystalline aliphatic polyester that consists of repeating units of five methylene groups and one ester group, which is degradable in the body [26]. PCL degradation products exert non-cytotoxic effects *in vivo* or *in vitro* [27,28]. A novel derivative of PCL, polycaprolactone methacryloyl (PCLMA), was applied to tissue engineering scaffolds by Elomaa [29]. After photocrosslinking, PCL showed excellent biocompatibility, biodegradability, and mechanical properties [29]. Subsequently, Elomaa et al. fabricated acellular human small intestine-mimicking tissue scaffolds using gelatin methacryloyl and PCLMA, which combined biocompatibility with high resolution [30]. PCL is typically used as the principal mechanical support for tissue in engineering bioscaffolds.

Recently, biodegradable metals have been used as GBR membranes [31]. Magnesium (Mg) performed well in terms of cell adhesion and osteogenic activity [32–34]. For example, Guo et al. fabricated a chitosan coated Mg alloy and found that it enhanced cell attachment and reduced the degradation rate of Mg [33]. The addition of Mg particles promoted cell proliferation and enhanced osteogenesis in novel PLGA scaffolds [35].

Herein, Col/PCLMA/Mg membranes were developed. The PCLMA was used to wrap the Col fibers for reinforcement, and to reduce Col degradation after photocrosslinking, while the Mg particles enhanced biocompatibility and osteogenic capability. After photocrosslinking, the mechanical and degradation properties, and biocompatibility of the Col/PCL/Mg membranes were assessed *in vitro* and *in vivo*.

## 2. Materials and methods

### 2.1. Materials

Polycaprolactone methacryloyl (PCLMA-3200) and the photoinitiator 2,4,6-trimethylbenzoyldiphenylphosphinate (TPO) were purchased from Engineering For Life (Suzhou, China). Absorbable Col membranes with smooth and coarse surfaces were purchased from Lando Biomaterials (Shenzhen, China).

### 2.2. Cell culture

Human gingival fibroblasts (HGFs) were purchased from Zhong Qiao Xin Zhou Biotechnology Co, Ltd. (Shanghai, China) and cultured with Dulbecco's modified Eagle's medium (DMEM; Gibco, USA). Human bone marrow mesenchymal stem cells (hBMSCs) were obtained from ScienCell (San Diego, CA, USA) and cultured in α-minimum essential medium (α-MEM; Gibco, USA). The proliferation medium (PM)

contained 10% (v/v) fetal bovine serum (FBS) and 1% (v/v) antibiotics. The osteogenic medium (OM) contained 10% (v/v) FBS, 1% (v/v) antibiotics, 10 nM dexamethasone, 200 μM ascorbic acid, and 10 mM β-glycerophosphate.

### 2.3. Preparation of membranes

Polycaprolactone methacryloyl was heated to 40°C and mixed with TPO at the ratio of 100: 0.5 (w/w) to form a homogeneous PCLMA/TPO solution. The mixture was evenly coated at 50 mg/cm$^2$ onto the smooth surface of the Col membranes, which were subsequently maintained at 37°C for 15 min to ensure complete infiltration of the PCLMA into the Col. To obtain a solid-like state, these membranes were maintained at 4°C for 10 min and then sterilized by cobalt-60 irradiation. Finally, the composite membranes were photocured using a 405-nm light source for subsequent tests. These photocrosslinked membranes were named Col/PCL. In the Col/PCL/Mg groups, Mg particles with a diameter of 75–150 μm were added to the homogeneous PCLMA solution at a ratio of 1: 20 (w/w), and repeatedly pipetted and vibrated for 30 min; the same procedures described above were then followed. For convenience, the PCLMA solution with TPO was directly photocured in the absence of the Col membrane in PCL groups. The controls were Col membranes without any processing.

### 2.4. Characterization of membranes

#### 2.4.1. Infrared spectroscopy

The compositions of the uncured and photocured membranes were analyzed by Fourier transform-infrared (FT-IR) spectroscopy (Nicolet iN10; Thermo Fisher Scientific, Waltham, MA, USA) in the range of 600–4000 cm$^{-1}$ for 256 scans.

#### 2.4.2. Morphology and elemental composition

The morphology of the smooth and coarse surfaces of membranes was examined by scanning electron microscopy (SEM; EVO 18; Zeiss, Oberkochen, Germany) with an accelerating voltage of 10 kV. All membranes were cut in the direction perpendicular to the smooth surface, and cross-sections were examined after sputter-coating with a thin layer of gold. Elemental analysis was performed using an energy dispersive spectrometer (INCA X-Act; Oxford Instruments, UK) attached to the SEM.

#### 2.4.3. Mechanical properties

Membranes with dimensions of 10 × 30 mm were fabricated for each group. In the tensile strength test, individual membranes were mounted into the grips with a gauge length of 15 mm and stretched at a crosshead speed of 5 mm/min until breaking. In the three-point flexure test, samples were placed in phosphate-buffered saline (PBS) and immersed *in vitro* at 37°C for 1 day to evaluate membrane stability. The immersed and initial membranes were placed on the test platform with a gauge length of 15 mm and compressed at 5 mm/min. The test continued until the membranes touched the third point. Stress-strain curves were acquired using an electronic universal testing machine (Z020; ZwickRoell, Ulm, Germany). The elastic modulus was calculated from the linear portion of the stress-strain curve.

#### 2.4.4. Swelling behavior

The membranes were lyophilized for about 24 h to obtain the dry weight (*Wd*). Subsequently, the lyophilized samples were immersed in PBS at room temperature for 24 h and 72 h to achieve a constant swelling weight (*Ws*). The swelling ratio was calculated according to the following equation:

$$\text{Swelling ratio} \ (\%) = \frac{Ws - Wd}{Wd} \times 100$$

### 2.5. Degradation behavior of membranes

#### 2.5.1. Degradation in vitro

The membranes were cut into squares of dimensions $10 \times 10$ mm and placed in the wells of a 24-well culture plate. The initial weights ($W0$) of the Col, PCL, Col/PCL, and Col/PCL/Mg membranes were determined. Then, they were immersed in PBS (pH=7.4) containing 28 units of collagenase (100 μg/mL). At preset time intervals (1, 4, 8, and 12 h, and 1, 3, 7, 14, 21, and 28 days), the enzyme activity was blocked by soaking the mixture in an ice bath. The residual moisture was removed by lyophilization. Then, the membranes were weighed to determine the mass change with time. The weight of the membranes at preset time intervals was called $Wt$. The mass change was calculated according to the following equation:

$$\text{Mass change } (\%) = \frac{Wt - W0}{W0} \times 100$$

Structural changes in the smooth and coarse surfaces of the Col, PCL, Col/PCL, and Col/PCL/Mg membranes were observed by SEM. The membranes were harvested after being immersed in PBS containing collagenase at preset time intervals and lyophilized before characterization by SEM.

To evaluate the concentration of released $Mg^{2+}$ ions, the membranes were soaked in simulated body fluid (SBF) (1 mL/6 cm$^2$) for 1, 3, 5, and 7 days. The resulting solutions were analyzed using inductively coupled plasma-optical emission spectroscopy (Optima 5300DV; PerkinElmer, Waltham, MA, USA).

#### 2.5.2. Degradation behavior in vivo

The animal assay was approved by the Peking University Health Science Center (Approval number: LA 2019019) following the protocol established by the Experimental Animal Ethics Committee. Twelve male Sprague-Dawley rats aged 8 weeks were randomly divided into four groups. They were anesthetized using pentobarbital sodium (50 mg/kg). The hair on the dorsal surface was shaved, and the skin was sterilized using iodophor cotton swabs. Then, an incision was made on the back and a 10-mm-diameter disc membrane was implanted subcutaneously in the dorsal pouches underneath the skin. Finally, the incision was closed and sterilized using iodophor cotton swabs. The initial weight of the membranes was measured ($W0$). Membranes were collected at week 8 post-surgery. The residual moisture was removed by lyophilization. Then, the membranes were weighed and observed by SEM.

### 2.6. Biocompatibility assessment in vitro

#### 2.6.1. Live/dead cell staining and cell attachment

Membranes were cut into discs 10 mm in diameter. The four types of membranes were placed in 24-well culture plates, and HGFs and hBMSCs were incubated on the surface of the membranes at a density of $8 \times 10^3$ cells/well, respectively. Subsequently, the cells were rinsed three times with PBS solution and incubated with 2 μM calcein-AM and 8 μM propidium iodide (Live/Dead Viability/Cytotoxicity Assay for Animal Cells; KeyGen Biotech Corp., Ltd., Nanjing, China) for 30 min at room temperature. The cells were then rinsed three times with PBS solution and visualized by laser scanning confocal microscopy (LSCM; LSM 710; Zeiss). Each sample was prepared in triplicate for observation.

For the cell attachment assay, HGFs and hBMSCs were incubated on the surface of the four types of membranes for 24 h and rinsed three times with PBS solution, respectively. Then, the cells were fixed with 4% paraformaldehyde for 30 min at room temperature, followed by permeabilization with 0.1% Triton X-100 in phosphate buffer for 7 min. The cells were then washed with PBS, followed by staining with 5 μg/mL FITC-conjugated phalloidin for 40 min and DAPI (Sigma, St. Louis, MO, USA) for 5 min; cells were then observed by LSCM. Meanwhile, SEM was used to observe cell morphology after the cells had incubated on the membrane surface for 24 h. Briefly, the cells were fixed with 4%

paraformaldehyde for 30 min, followed by washing with PBS, and dehydrated (by gradient dehydration) from 50% to absolute ethanol. Samples were imaged by SEM after coating with a thin layer of gold.

#### 2.6.2. Cell proliferation

The membranes were cut into discs 6 mm in diameter. HGFs were cultured in the same environment as for the live/dead cell staining assay. The four types of membranes were placed in 96-well culture plates and the HGFs were incubated on the surface of the membranes at a density of $3 \times 10^3$ cells/well. After incubating for 1, 3, 5, and 7 days, cell proliferation was determined using a Cell Counting Kit-8 (CCK-8; Dojindo, Kumamoto, Japan). The spectrophotometric absorbance of each well was measured using a microplate reader (ELx808; Biotek, Winooski, VT, USA) at 450 nm. Each group was tested in triplicate. The cell proliferation rate was calculated according to the following equation:

$$\text{Cell proliferation } (\%) = \frac{OD - OD(blank)}{OD(Col) - OD(blank)} \times 100$$

### 2.7. Osteogenic efficiency in vitro

#### 2.7.1. Alkaline phosphatase (ALP) staining and ALP activity of hBMSCs

The membranes were immersed in the OM and PM for 24 h at 37°C, respectively. The hBMSCs were seeded on 6-well plates at a density of $2 \times 10^6$ cells/mL and were cultured by corresponding extracts, which were divided into five groups as follows: (1) Blank, (2) Col, (3) PCL, (4) Col/PCL, and (5) Col/PCL/Mg. The ALP staining was conducted using the nitroblue tetrazolium/5-bromo-4-chloro-3-indolyl phosphate staining kit (CoWin Biotech, China) after culturing by PM and OM, respectively. The ALP activity was quantified at the same time point. Before measuring the total protein content using the BCA protein assay kit (Thermo Fisher Scientific, USA), these cells were lysed by 1% Triton X-100 for 30 min. ALP activity was measured by using the ALP activity assay kit (Nanjing Jiancheng Institute of Biological Engineering). Absorbance was measured at 520 nm, and the ALP activity was calculated.

#### 2.7.2. Real-time quantitative PCR (RT-qPCR)

Total cellular RNA was extracted from hBMSCs cultured in proliferation and osteogenic medium for 7 and 14 days with TRIzol reagent (Invitrogen, Carlsbad, CA, USA). PrimeScript RT Reagent Kit (Takara, Tokyo, Japan) was used to synthesize the cDNA. RT-qPCR was conducted with SYBR Green Master Mix on an ABI Prism 7500 real-time PCR System. Gene expression was normalized to the expression of GAPDH, which was used as the reference gene. The primer sequences of human GAPDH, RUNX2, ALP, OCN, and OSX are in Table 1.

### 2.8. Osteogenic efficiency in bone defects

The animal assay was approved by the Peking University Health Science Center (Approval number: LA 2019019) following the protocol established by the Experimental Animal Ethics Committee. Twenty-five male Sprague-Dawley rats aged 8 weeks were randomly divided into the following five groups (n = 5): blank control (bone defects without membrane), Col membranes, PCL membranes, Col/PCL membranes, and

**Table 1**
Primer sequences for RT-PCR.

| Target gene | Forward Primer ( 5'-3' ) | Reverse Primer ( 3'-5' ) |
|---|---|---|
| GAPDH | AAGGTCGGAGTCAACGGATTTG | TCCTGGAAGATGGTGATGGGAT |
| ALP | ATGGGGATGGGTGTCTCCACA | CCACGAAGGGGAACTTGTC |
| OCN | AGCCACCGAGACACCATGAGA | GGCTGCACCTTTGCTGGACT |
| OSX | ACTGCCCCACCCCTTAGACA | GAGGTGCACCCCCAAACCAA |
| RUNX2 | ACTACCAGCCACCGAGACCA | ACTGCTTGCAGCCTTAAATGACTCT |

Col/PCL/Mg membranes. They were anesthetized with pentobarbital sodium (50 mg/kg) to minimize suffering. Testing was conducted as described previously [36]. On the right side of each rat's calvaria, a 6-mm-diameter, full-thickness critical-sized defect was prepared with a trephine bur. The 8-mm-diameter PCL membranes, cured in advance, were then implanted into the defects, while the Col/PCLMA and Col/PCLMA/Mg membranes were placed into the defects and photocured for 30 s. Finally, the incision was closed and all rats were cultured in an environmentally controlled animal care facility.

All rats were sacrificed under anesthesia 8 weeks after surgery. The calvaria, including the implanted membranes and main organs (heart, liver, spleen, lung, and kidney), of the animals, were carefully collected and then fixed in 10% neutral buffered formalin for 72 h. The new bone formation within the bone defect was observed using a high-resolution Inveon instrument (Siemens, Munich, Germany). Three-dimensional (3D) visualization software (Inveon Research Workplace; Siemens , Munich, Germany) was used for 3D reconstruction of the images at an effective pixel size of 18.428 μm. New bone volume in the defects was determined by quantifying the pixels in the images.

Then, the samples were decalcified for 21 days in 10% EDTA solution (pH 7.4), under constant shaking at room temperature. Specimens were then embedded in paraffin and sliced into 5-μm-thick serial sections. The main organs were also fixed, dehydrated, embedded, and sliced. Hematoxylin-eosin (H&E), Masson, and immunohistochemical (IHC)

staining were performed for histological examination. Images of the sections were obtained using an optical microscope (BX51; Olympus, Tokyo, Japan).

### 2.9. Statistical analysis

The results are expressed as mean ± standard deviation. The groups were compared by one-way ANOVA using SPSS 21.0 software (SPSS Inc., Chicago, IL, USA). A significance level of 5% was used for all tests.

## 3. Results

### 3.1. Fabrication process and mechanism

Polycaprolactone methacryloyl has a solid-like state and resembles wax at room temperature, but is in a fluid liquid state above 37°C. The PCLMA completely infiltrated the smooth and coarse Col membrane surfaces at 40°C. After photocuring, PCL and Col bonded tightly and formed an interpenetrating polymer network resembling that of steel-reinforced concrete (Fig. 1C).

### 3.2. Characterization of composite membranes

The composition of the composite membranes was qualitatively
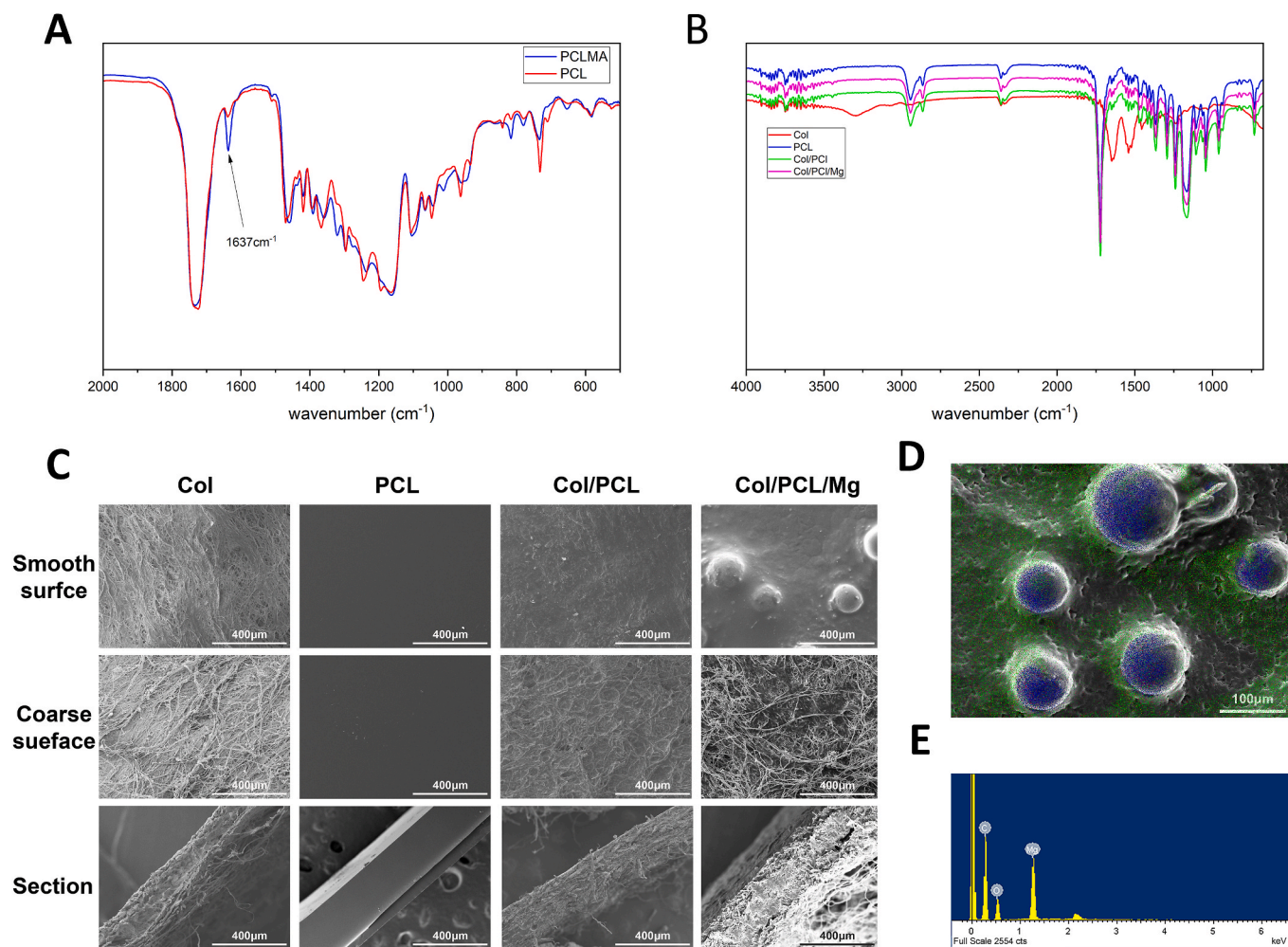


**Fig. 1.** Formulation and characterization of the photocrosslinkable composite membranes. Fourier transform infrared spectra of (A) PCLMA and photocrosslinked PCL, and (B) Col, PCL, Col/PCL, and Col/PCL/Mg membranes. (C) Scanning electron microscopy images showing the morphology of Col, PCL, Col/PCL, and Col/PCL/Mg membranes. Energy dispersive spectrometry (D) maps and (E) spectra of Col/PCL/Mg membranes; red, green, and blue colors represent elemental O, C, and Mg, respectively.

determined by FT-IR spectroscopy (Fig. 1A and B). For the photocured membranes, the reduced intensity of the amide I peak at 1638 cm$^{-1}$ distinguished them from the uncured membranes. The spectra of the composite membranes and PCL were similar, and differed from that of the Col membranes.

The thickness of the Col, PCL, Col/PCL, and Col/PCL/Mg membranes was 300–600 μm. Fig. 1C presents SEM micrographs of the smooth and coarse surfaces and cross-sections. The Col fibers on the coarse surface of the Col membranes were visible and appeared more linear, while they were denser on the smooth surface. The PCL and Col/PCL groups had comparatively smooth surfaces free of Col fibers. In the Col/PCL and Col/PCL/Mg groups, PCL filled the interfibrillar spaces between the Col fibrils on coarse surfaces and sections. Notably, Mg particles were distributed homogenously on the smooth surfaces of Col/PCL/Mg membranes, and energy-dispersive spectrometry mapping revealed that PCL covered the Mg particles (Fig. 1D and E).

### 3.3. Mechanical properties

The elastic modulus of the PCL membranes was the lowest, and that of Col/PCL was the highest, at 454.97±43.84 MPa, in the four groups (Fig. 2A). The incorporation of Mg particles into the Col/PCL/Mg membranes decreased the elastic modulus (P > 0.05). During the flexure test, the elastic modulus of the PCL membranes was even lower than that of the Col membranes in the non-immersed state (P < 0.05) (Fig. 2B). The stress-strain curves (Fig. 2D) showed that the maximum strength of the Col/PCL and Col/PCL/Mg membranes was much higher than those of the other groups. After immersion in PBS, the modulus of the Col/PCL and Col/PCL/Mg membranes was much higher than that of the Col membranes after immersion (P < 0.05) (Fig. 2C). The Col membranes completely lost their supportive properties, which were unmeasurable, while the other three groups showed similar stress-strain curves

(Fig. 2E).

### 3.4. Swelling behavior

Swelling ratio data are presented in Fig. 2F. The Col membranes absorbed two- and three-times their weight after immersion for 24 h and 72 h, respectively (P < 0.05). The PCL membranes showed no weight change after immersion. The water absorption of Col/PCL and Col/PCL/Mg membranes lay between that of the Col and PCL ones, and was unchanged after immersion for 24 h and 72 h (P > 0.05).

### 3.5. Degradation behavior of membranes in vitro

Fig. 3A and B shows the morphological changes of the smooth and coarse surfaces during the entire degradation process. The Col membranes became steadily looser, and the Col fibers steadily smaller, before almost complete degradation on day 7. The smooth surfaces of the PCL and Col/PCL membranes were virtually unchanged according to SEM observations. However, in the Col/PCL/Mg group, some of the Mg particles shed from the smooth surface and small pits were evident. Interestingly, the coarse surfaces of the Col/PCL and Col/PCL/Mg membranes were clearly altered: the appearance of the Col fibers gradually blurred from week 1 and disappeared at week 4, leaving cracks in the coarse surfaces. Fig. 3C presents the mass change of the membranes *in vitro*. Degradation of the Col membranes was notably faster than those of the other three types of membranes; Col membranes were completely degraded on day 7. In contrast, almost no PCL membranes degraded after immersion in PBS containing collagenase for 4 weeks. The Col/PCL and Col/PCL/Mg membranes degraded by about 12% and 8%, respectively, after 4 weeks.

The concentration of Mg$^{2+}$ ions in the Col, PCL, and Col/PCL groups maintained at 30 mg/L, which was the basal concentrations of SBF,
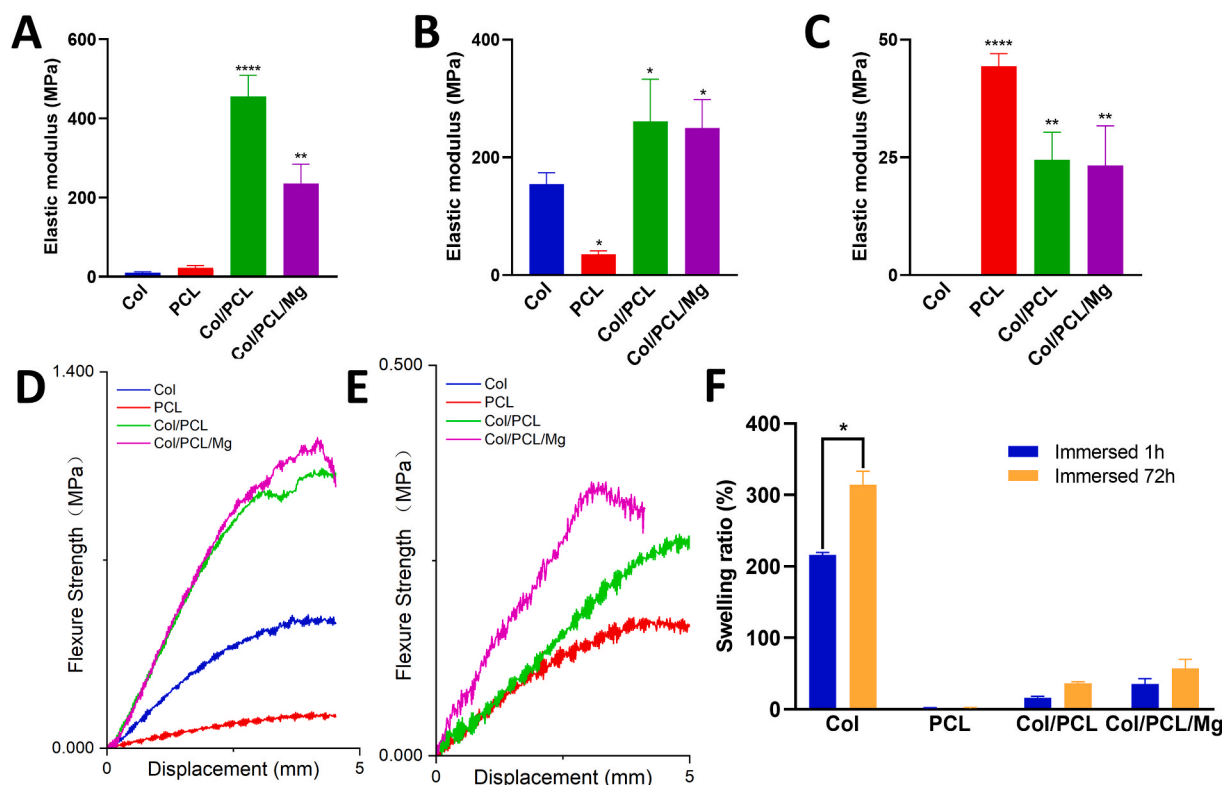


**Fig. 2.** Mechanical properties and Swelling behavior of the photocrosslinked composite membranes. (A) Elastic modulus derived from tensile testing of Col, PCL, Col/PCL, and Col/PCL/Mg membranes. Elastic moduli from flexure testing of the (B) original membranes and (C) membranes immersed in PBS for 1 day. Stress–strain curves derived from flexure testing of the (D) original membranes and (E) membranes immersed in PBS for 1 day. (F) Swelling behavior of Col, PCL, Col/PCL, and Col/PCL/Mg membranes. (*p < 0.05, **p < 0.01, ***p < 0.001, ****p < 0.0001 when compared with Col group).
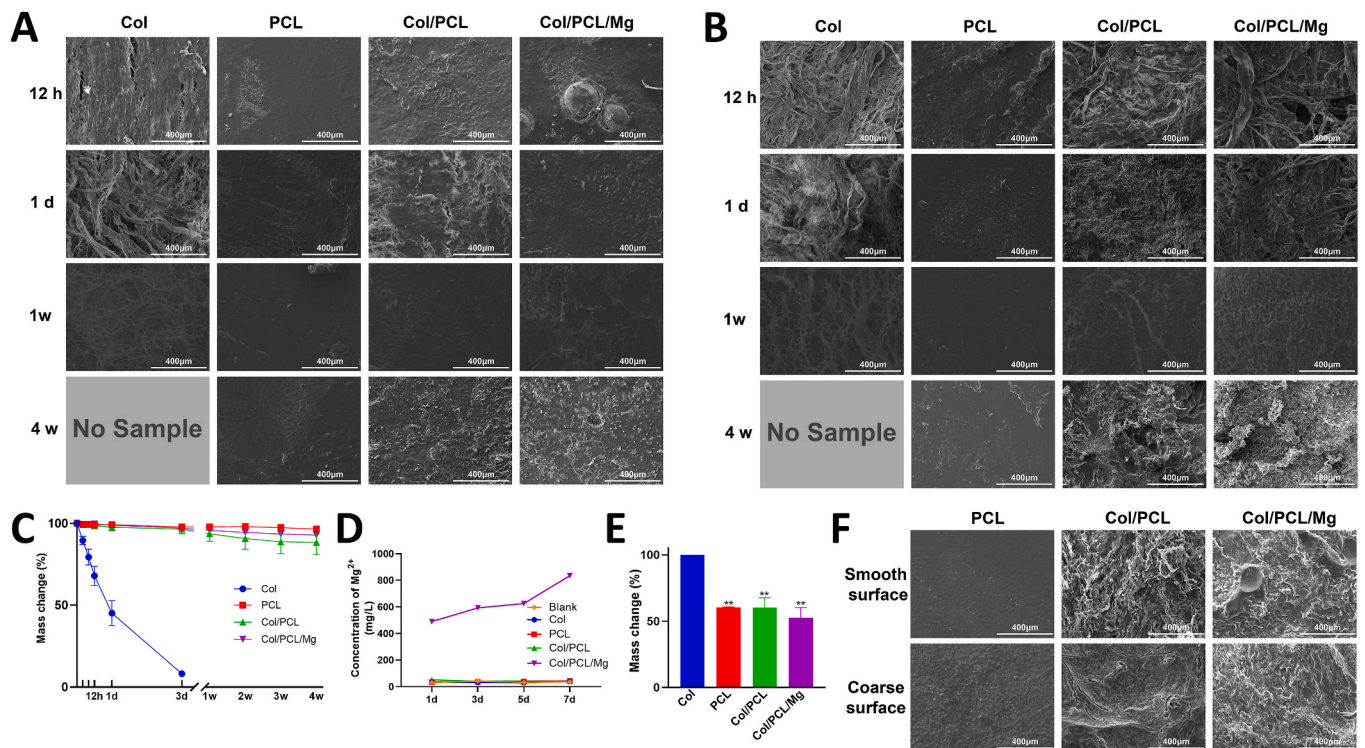
**Fig. 3.** Degradation behavior of membranes *in vivo* and *in vitro*. Scanning electron microscopy morphologies of (A) smooth and (B) coarse surfaces of Col, PCL, Col/PCL, and Col/PCL/Mg membranes after immersion in PBS containing collagenase for 12 h, 1 day, 1 week, and 4 weeks, and the corresponding mass changes of these membranes (C) *in vitro* and (E) *in vivo*. (D) Concentration of Mg2+ ions after soaking Col, PCL, Col/PCL, and Col/PCL/Mg membranes in simulated body fluid for 1, 3, 5, and 7 days. (F) Scanning electron microscopy morphologies of smooth and coarse surfaces of Col, PCL, Col/PCL, and Col/PCL/Mg membranes after implantation into subcutaneous tissue for 8 weeks (**p < 0.01 when compared with Col group).

while release from the SBF-immersed Col/PCL/Mg group gradually increased from 490.30 to 846.67 mg/L from day 1–7 (Fig. 3D).

### 3.6. Degradation behavior of membranes in vivo

The mass changes are shown in Fig. 3E. The Col membranes were completely degraded after 8 weeks of implantation. In contrast, the weights of the PCL, Col/PCL, and Col/PCL/Mg membranes over this period decreased by 50%, which corresponded approximately to the weight of Col; SEM images confirmed these findings. Collagen fibers had completely disappeared, and cracks were observed in the coarse surface of the Col/PCL and Col/PCL/Mg membranes. Interestingly, the smooth surface of the Col/PCL/Mg membrane changed significantly; Mg particles had disappeared completely and small pits were evident on the surface (Fig. 3F).

### 3.7. Biocompatibility assessment

Fig. 4 presents the biocompatibility assay results. The live/dead cell stains assay revealed only a few dead HGFs on the Col membranes, and no dead HGFs were observed on the other three types of membranes after 24 h of incubation (Fig. 4A). Notably, the HGFs in the Col/PCL/Mg group demonstrated increased proliferative potential. No dead hBMSCs were observed on four types of membranes (Fig. 4D). Concerning cell attachment, LSCM images showed spindle-shaped HGFs that were scattered across the membrane surfaces in all four groups. SEM imaging revealed stretched HGF pseudopods in the Col/PCL/Mg group (Fig. 4B). The same results were also observed in hBMSCs (Fig. 4E). Finally, the cell proliferation rate revealed a similar proliferation potential of the HGFs in all groups (P > 0.05) (Fig. 4C).

### 3.8. Osteogenic efficiency in vitro

The ALP staining showed that the extract OM of Col/PCL/Mg membranes enhanced osteogenesis (Fig. 5A). The quantification of ALP activity also performed that the extract OM of Col/PCL/Mg membranes significantly enhanced osteogenic potential than other extracts (Fig. 5B). We also analyzed the mRNA expression of ALP, and the Col/PCL/Mg groups exhibited a 4-fold increase in expression compared with other groups (Fig. 5C). Consistent with these findings, the extract OM of Col/PCL/Mg membranes led to enhanced mRNA expression of RUNX2, OCN, and OSX on days 14, respectively (Fig. 5D–F).

### 3.9. Osteogenic efficiency in vivo

After 8 weeks, the defective bone was harvested and morphological changes were observed by micro-computed tomography (micro-CT) and examination of tissue slices (Fig. 6A). Visual inspection revealed that the defects in Col membranes were completely replaced by a thin layer of new bone. There was a small amount of unhealed defect remaining in the other three groups. However, micro-CT images confirmed that the new bone in the PCL, Col/PCL, and Col/PCL/Mg groups was more than in the Col group. Bone mineral density (BMD) analysis and total bone volume (BV) measurements indicated similar trends, with the largest values found in the Col/PCL/Mg group (P < 0.05) (Fig. 6C and D). H&E staining of slices indicated that cells and new bone-like tissue were distributed on the bone defects in the Col, PCL, Col/PCL, and Col/PCL/Mg groups. In the Col/PCL/Mg group, there was more eosinophilic new bone-like tissue in layers. Likewise, except for the blank groups, collagen (stained blue) was observed in almost all groups. More collagen, in a cord-like arrangement, was observed in the Col/PCL and Col/PCL/Mg groups. In addition, IHC staining of OCN presented the same trend (Fig. 6B). H&E staining of slices of the main organs, including heart,
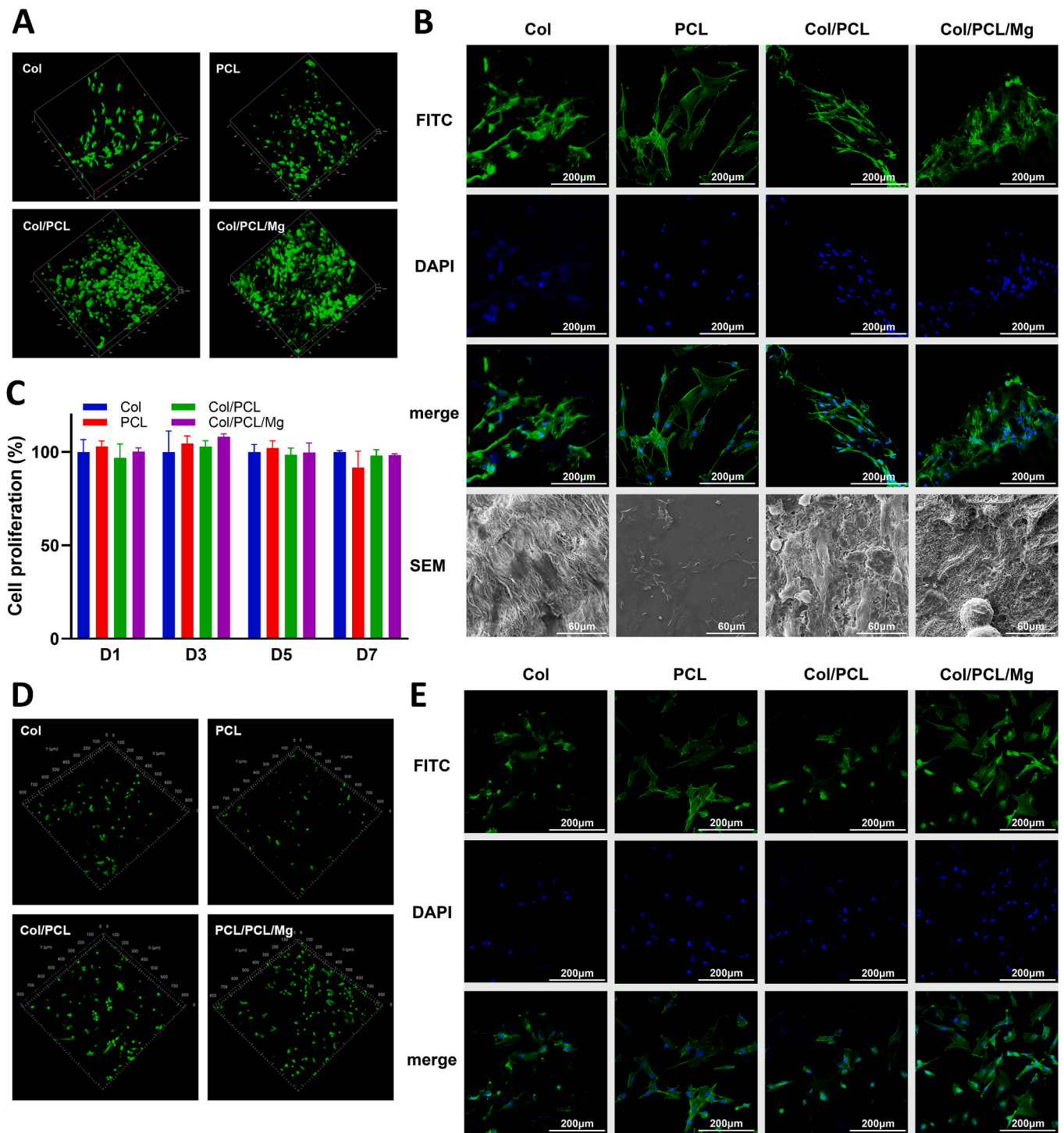
**Fig. 4.** Biocompatibility assessment. (A) Live/dead cell staining of HGFs. The red cells represent dead cells and the green represent live cells. (B) Attachment of HGFs to Col, PCL, Col/PCL, and Col/PCL/Mg membranes observed by LSCM and SEM. (C) Cell proliferation values of HGFs obtained using the Counting Kit 8 on days 1, 3, 5, and 7 in each group. (D) Live/dead cell staining of hBMSCs. The red cells represent dead cells and the green represent live cells. (E) Attachment of hBMSCs to Col, PCL, Col/PCL, and Col/PCL/Mg membranes observed by LSCM.

liver, spleen, lung, and kidney, indicated no obvious inflammatory cell infiltration in all groups (Supplement 1).

## 4. Discussion

Typically, GBR is used to vertically and horizontally reconstruct bone, and many strategies have been developed to allow GBR membranes to induce more bone regeneration [5,6,17]. In this study, PCL

was used to reinforce Col membranes [37], and Mg particles were used to enhance the biocompatibility of the membranes. The photo-crosslinkable Col/PCL/Mg membranes were successfully fabricated and used to repair calvaria defects of rats *in vivo*.

During clinical application, the Col membranes immediately lost the support of their Col fibers, and readily collapsed after immersion in water or blood. An ideal membrane should have sufficient stiffness to create and maintain a suitable space for the intended osseous
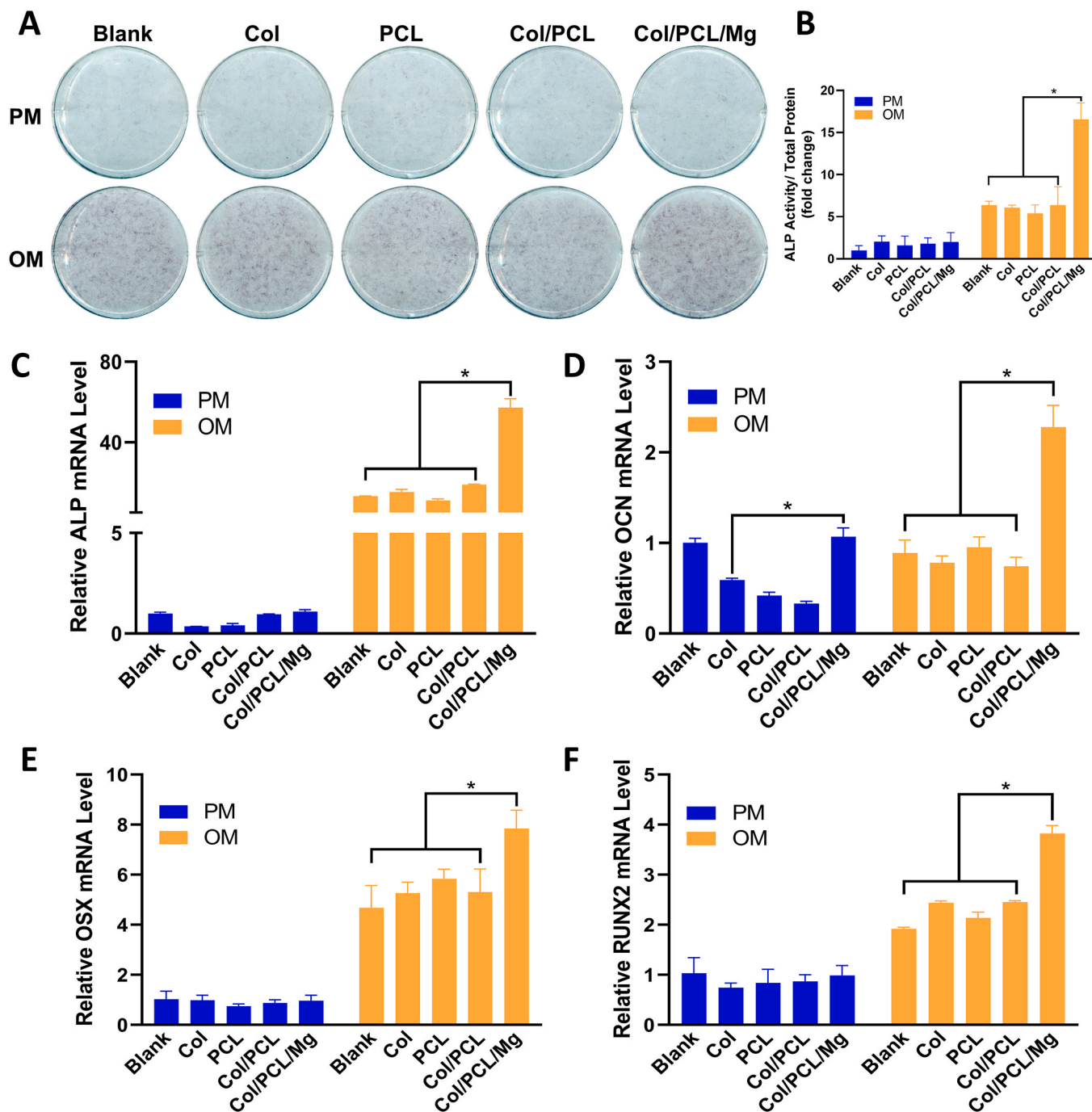
**Fig. 5.** Osteogenic efficiency *in vitro*. (A) Alkaline phosphatase activity and (B) quantitative alkaline phosphatase assay (n = 3) after the hBMSCs were cultured in extracts for 7 days; Evaluating osteogenic differentiation of hBMSCs cultured in extract liquid by analyzing relative expressions of genes in relation to osteogenic differentiation: (C) ALP; (D) OCN; (E) OSX; (F) RUNX2. (*$p < 0.05$, n = 3).

regeneration [18]. Titanium mesh is typically used to achieve this goal in the clinic. First, the plasticity of Ti mesh permits bending, contouring, and adaptation to any unique bony defect [38]. In this study, before photocuring, the Col/PCLMA and Col/PCLMA/Mg membranes displayed high plasticity and could be bent to fit the morphology of the bone defect, or to reconstruct the ideal bone shape. The photocrosslinked Col/PCL and Col/PCL/Mg membranes had stiffness similar to that of Ti mesh, and could prevent contour collapse and mucosal compression. Although other photocrosslinkable materials for GBR have been developed, such as GelMA/PEGDA [39] and methacrylated gelatin/nanohydroxyapatite/poly (L-lactic acid) [40], they are photocrosslinked before clinical use. In contrast, the Col/PCLMA and

Col/PCLMA/Mg membranes in this study showed excellent clinical manageability.

Titanium mesh has excellent mechanical properties promoting the stabilization of bone grafts. Bai et al. prepared 3D-printed Ti meshes, with a maximum bending strength of 178.00±20.99 MPa at 0.3 mm in thickness and 5 mm in diameter [41]. Although Fig. 2D and E showed that these composite membranes could not reach the same flexure strength because of the properties of PCL and collagen themself, Fig. 2A and B shows that the elastic modulus of the Col/PCL membranes increased by approximately 50% than that of collagen membranes and maintain a certain strength *in vivo* environment. Theoretically, these properties could be further improved by increasing membrane
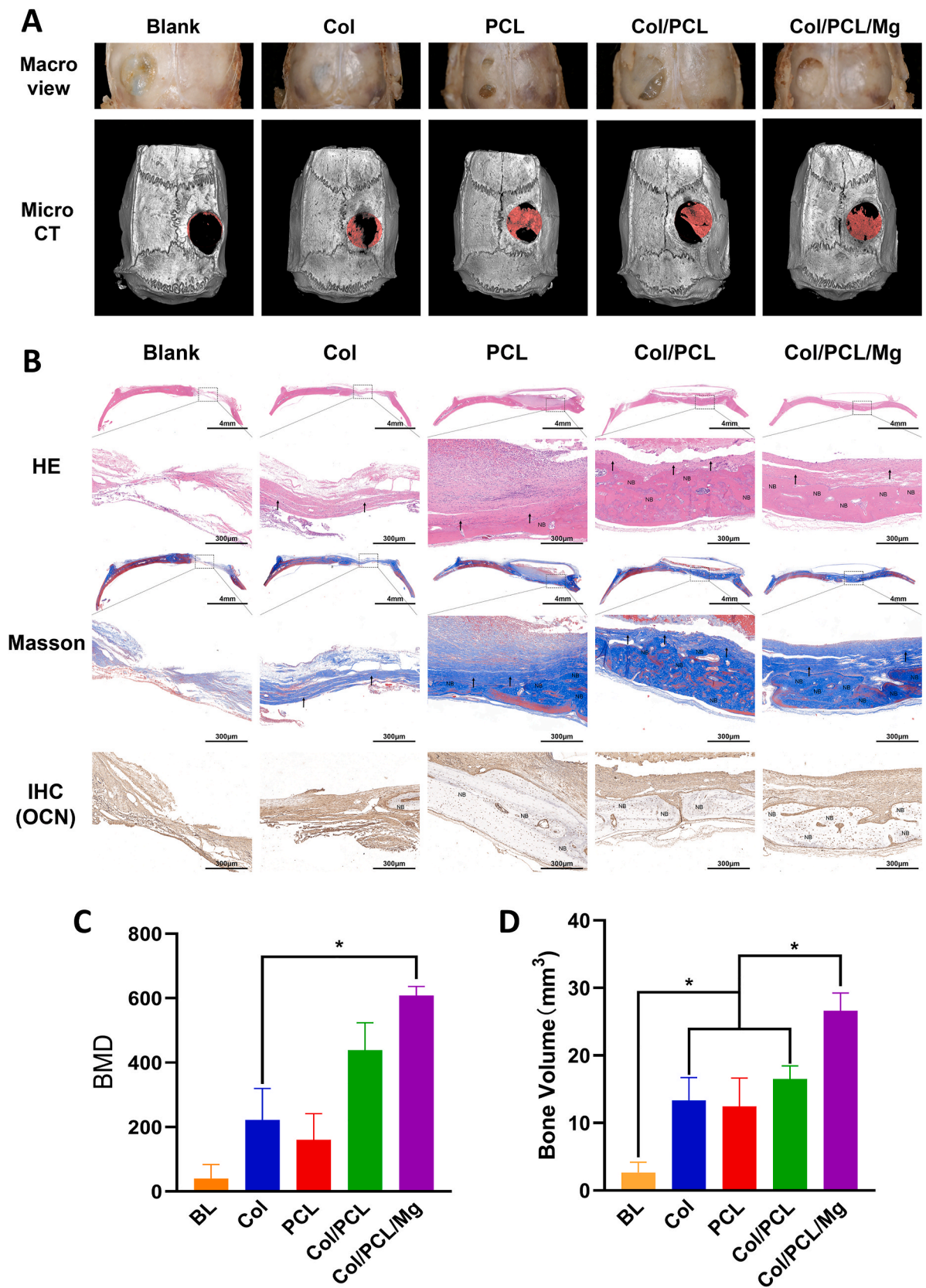
**Fig. 6.** Osteogenic efficiency *in vivo*. (A) Macro and micro CT images of new bone regeneration. (B) Hematoxylin–eosin, Masson, and immunohistochemical (IHC) staining of blank control, Col, PCL, Col/PCL, and Col/PCL/Mg groups after implantation into calvaria defects for 8 weeks. NB represents eosinophilic new bone like tissue, ↑ represents collagen; (C) Bone mineral density of each group after reconstruction of micro CT images. (D) BV of each group after reconstruction of micro CT images. (*$p < 0.05$, n = 5).

thickness. Via electrospinning, Jin et al. fabricated a fish Col- and nanohydroxyapatite-enhanced poly (lactide-*co*-glycolide) nanofibrous membrane with an elastic modulus of 124.3±22.7 MPa during tensile testing [42]. In this study, the elastic modulus of the Col/PCL and Col/PCL/Mg membranes was determined by tensile testing as 312.50±27.47 and 241.3±19.10 MPa, respectively. Similar to the present study, PCL was used in kind of scaffold because of its great mechanical properties, such as gelatin containing PCL conduits [43], PCL/β-TCP cross-scale scaffold [44].

It has been suggested that an ideal GBR membrane should preserve its barrier function for 16–24 weeks [23] and remain in the bone defect for 1 month for every mm of bone regeneration [24]. However, the degradation time of commercial Col membranes varies greatly (range: 4–38 weeks) [18,20]. The Col membranes used in this study were porcine natural Col. The membranes degraded 90% by collagenase after only 3 days, but the Col fiber in the Col/PCL and Col/PCL/Mg membranes remained intact for 4 weeks *in vitro* due to the interpenetrating polymer networks of PCL and Col (Fig. 3C). The degradation assay *in vivo* showed the same trend (Fig. 3E). Further *in vivo* testing is needed to establish the time to complete the degradation of these membranes.

Collagen membranes are commonly used in the clinical setting and show good cytocompatibility [45] and relatively high bone augmentation [46]. Therefore, we selected Col as the basic material in this research. In addition, the application of Mg particles resulted in excellent biocompatibility and osteogenesis. Fig. 4B shows extensive cell attachment, and Figs. 5 and 6 the obvious osteogenic potential, in the Col/PCL/Mg group. Previous research demonstrated that Mg alloys promoted bone regeneration with good biocompatibility [47,48]. Ahmadi et al. fabricated polycaprolactone fumarate/gelatin membranes containing 5 wt% Si and Mg codoped fluorapatite nanoparticles that displayed appropriate biological properties [49]. The Mg particles reacted with water to produce $Mg(OH)_2$ [31]. Fig. 3D shows that the concentration of $Mg^{2+}$ ions in the Col/PCL/Mg group was higher than in other groups. Higher local pH could promote the formation of calcium phosphate compounds, which contribute to the formation of new bone [50]. Hung et al. verified that the role of magnesium ions in bone regeneration involves the canonical wnt signaling pathway through wnt3a [51]. It was also reported that magnesium ions could induce stem cell osteogenic differentiation by selectively activated MAPK/ERK pathways or upregulating the expression of COL10A1 and vascular endothelial growth factor [52]. Other research found that magnesium could promote bone healing by calcitonin gene-related polypeptide-α mediated osteogenic differentiation [53].

One drawback of Mg alloys is rapid and uncontrollable degradation [54]. Many strategies using polymeric coatings have been developed to address this issue [55]. PCL is a promising coating material candidate to control the degradation rate [55]. Chen et al. coated high-purity Mg with PCL and PLA, and found that the polymeric coating improved corrosion resistance and degradation [56]. Analogously, herein, Mg particles enhanced the biocompatibility and osteogenesis potential of PCL, while PCL slowed down the degradation of Mg.

## 5. Conclusion

The developed photocrosslinkable Col/PCL/Mg membranes exhibited excellent clinical manageability. The photocrosslinked membranes displayed superior mechanical properties and excellent biocompatibility, and can serve as an alternative to conventional GBR membranes in guided bone regeneration.

## CRediT authorship contribution statement

**Feilong Wang:** Conceptualization, Writing – original draft, Resources. **Dandan Xia:** Methodology, Data curation, Writing – review & editing. **Siyi Wang:** Formal analysis, Investigation. **Ranli Gu:** Formal analysis, Validation. **Fan Yang:** Investigation, Resources. **Xiao Zhao:**

Software, Resources. **Xuenan Liu:** Validation, Data curation. **Yuan Zhu:** Validation, Software. **Hao Liu:** Methodology, Software. **Yongxiang Xu:** Conceptualization, Project administration, Funding acquisition. **Yunsong Liu:** Methodology, Project administration, Funding acquisition. **Yongsheng Zhou:** Supervision.

## Appendix A. Supplementary data

Supplementary data to this article can be found online at https://doi.org/10.1016/j.bioactmat.2021.10.019.

## Declaration of competing interest

The authors declared that they have no conflicts of interest to this paper. We declare that we do not have any commercial or associative interest that represents a conflict of interest in connection with this paper.

## References

[1] H. Zhang, J. Shan, P. Zhang, X. Chen, H. Jiang, Trabeculae microstructure parameters serve as effective predictors for marginal bone loss of dental implant in the mandible, Sci. Rep. 10 (1) (2020) 18437, https://doi.org/10.1038/s41598-020-75563-y.
[2] O. Moses, S. Pitaru, Z. Artzi, C.E. Nemcovsky, Healing of dehiscence-type defects in implants placed together with different barrier membranes: a comparative clinical study, Clin. Oral Implants Res. 16 (2) (2005) 210–219, https://doi.org/10.1111/j.1600-0501.2004.01100.x.
[3] J.Y. Lee, J. Lee, Y.K. Kim, Comparative analysis of guided bone regeneration using autogenous tooth bone graft material with and without resorbable membrane, J. Dent. Sci. 8 (3) (2013) 281–286, https://doi.org/10.1016/j.jds.2013.03.001.
[4] C.H.F. Hämmerle, R.E. Jung, A. Feloutzis, A systematic review of the survival of implants in bone sites augmented with barrier membranes (guided bone regeneration) in partially edentulous patients, J. Clin. Periodontol. 29 (Suppl 3) (2002) 226–233, https://doi.org/10.1034/j.1600-051x.29.s3.14.x.
[5] P. Aprile, D. Letourneur, T. Simon-Yarza, Membranes for guided bone regeneration: a road from bench to bedside, Adv Healthc Mater 9 (19) (2020), e2000707, https://doi.org/10.1002/adhm.202000707.
[6] O. Omar, I. Elgali, C. Dahlin, P. Thomsen, Barrier membranes: more than the barrier effect? J. Clin. Periodontol. 46 (Suppl 21) (2019) 103–123, https://doi.org/10.1111/jcpe.13068.
[7] C. Dahlin, A. Linde, J. Gottlow, S. Nyman, Healing of bone defects by guided tissue regeneration, Plast. Reconstr. Surg. 81 (5) (1988) 672–676, https://doi.org/10.1097/00006534-198805000-00004.
[8] J. Gottlow, Guided tissue regeneration using bioresorbable and non-resorbable devices - initial healing and long-term results, J. Periodontol. 64 (11) (1993) 1157–1165, https://doi.org/10.1902/jop.1993.64.11s.1157.
[9] R. Dimitriou, G.I. Mataliotakis, G.M. Calori, P.V. Giannoudis, The role of barrier membranes for guided bone regeneration and restoration of large bone defects: current experimental and clinical evidence, BMC Med. 10 (2012) 24, https://doi.org/10.1186/1741-7015-10-81.
[10] D.F. Williams, Biocompatibility pathways: biomaterials-induced sterile inflammation, mechanotransduction, and principles of biocompatibility control, ACS Biomater. Sci. Eng. 3 (1) (2017) 2–35, https://doi.org/10.1021/acsbiomaterials.6b00607.
[11] M. Sanz, C. Dahlin, D. Apatzidou, Z. Artzi, D. Bozic, E. Calciolari, H. De Bruyn, H. Dommisch, N. Donos, P. Eickholz, J.E. Ellingsen, H.J. Haugen, D. Herrera, F. Lambert, P. Layrolle, E. Montero, K. Mustafa, O. Omar, H. Schliephake, Biomaterials and regenerative technologies used in bone regeneration in the craniomaxillofacial region: consensus report of group 2 of the 15th european workshop on periodontology on bone regeneration, J. Clin. Periodontol. 46 (Suppl 21) (2019) 82–91, https://doi.org/10.1111/jcpe.13123.
[12] L. Sbricoli, R. Guazzo, M. Annunziata, L. Gobbato, E. Bressan, L. Nastri, Selection of collagen membranes for bone regeneration: a literature review, Materials 13 (3) (2020) 786, https://doi.org/10.3390/ma13030786.
[13] A. Turri, I. Elgali, F. Vazirisani, A. Johansson, L. Emanuelsson, C. Dahlin, P. Thomsen, O. Omar, Guided bone regeneration is promoted by the molecular events in the membrane compartment, Biomaterials 84 (2016) 167–183, https://doi.org/10.1016/j.biomaterials.2016.01.034.
[14] L.L. Lima, P.F. Gonçalves, E.A. Sallum, M.Z. Casati, F.H. Nociti, Guided tissue regeneration may modulate gene expression in periodontal intrabony defects: a

human study, J. Periodontal. Res. 43 (4) (2008) 459–464, https://doi.org/10.1111/j.1600-0765.2008.01094.x.

[15] A. Cucchi, E. Vignudelli, A. Napolitano, C. Marchetti, G. Corinaldesi, Evaluation of complication rates and vertical bone gain after guided bone regeneration with non-resorbable membranes versus titanium meshes and resorbable membranes. A randomized clinical trial, Clin. Implant Dent. Relat. Res. 19 (5) (2017) 821–832, https://doi.org/10.1111/cid.12520.

[16] W. Li, Y. Ding, S. Yu, Q. Yao, A.R. Boccaccini, Multifunctional chitosan-45s5 bioactive glass-poly(3-hydroxybutyrate-co-3-hydroxyvalerate) microsphere composite membranes for guided tissue/bone regeneration, ACS Appl. Mater. Interfaces 7 (37) (2015) 20845–20854, https://doi.org/10.1021/acsami.5b06128.

[17] D. Abdelaziz, A. Hefnawy, E. Al-Wakeel, A. El-Fallal, I.M. El-Sherbiny, New biodegradable nanoparticles-in-nanofibers based membranes for guided periodontal tissue and bone regeneration with enhanced antibacterial activity, J. Adv. Res. 28 (2021) 51–62, https://doi.org/10.1016/j.jare.2020.06.014.

[18] Y.D. Rakhmatia, Y. Ayukawa, A. Furuhashi, K. Koyano, Current barrier membranes: titanium mesh and other membranes for guided bone regeneration in dental applications, J Prosthodont Res 57 (1) (2013) 3–14, https://doi.org/10.1016/j.jpor.2012.12.001.

[19] M. Meyer, Processing of collagen based biomaterials and the resulting materials properties, Biomed. Eng. Online 18 (1) (2019), https://doi.org/10.1186/s12938-019-0647-0, 24-24.

[20] E. Calciolari, F. Ravanetti, A. Strange, N. Mardas, L. Bozec, A. Cacchioli, N. Kostomitsopoulos, N. Donos, Degradation pattern of a porcine collagen membrane in an in vivo model of guided bone regeneration, J. Periodontal. Res. 53 (3) (2018) 430–439, https://doi.org/10.1111/jre.12530.

[21] O. Moses, D. Vitrial, G. Aboodi, A. Sculean, H. Tal, A. Kozlovsky, Z. Artzi, M. Weinreb, C.E. Nemcovsky, Biodegradation of three different collagen membranes in the rat calvarium: a comparative study, J. Periodontol. 79 (5) (2008) 905–911, https://doi.org/10.1902/jop.2008.070361.

[22] M. Atef, A. Tarek, M. Shaheen, R.M. Alarawi, N. Askar, Horizontal ridge augmentation using native collagen membrane vs titanium mesh in atrophic maxillary ridges: randomized clinical trial, Clin. Implant Dent. Relat. Res. 22 (2) (2020) 156–166, https://doi.org/10.1111/cid.12892.

[23] A. Bharadwaz, A.C. Jayasuriya, Recent trends in the application of widely used natural and synthetic polymer nanocomposites in bone tissue regeneration, Mater Sci Eng C Mater Biol Appl 110 (2020) 110698, https://doi.org/10.1016/j.msec.2020.110698.

[24] A.A. Chaudhari, K. Vig, D.R. Baganizi, R. Sahu, S. Dixit, V. Dennis, S.R. Singh, S.R. Pillai, Future prospects for scaffolding methods and biomaterials in skin tissue engineering: a review, Int. J. Mol. Sci. 17 (12) (2016) 1974, https://doi.org/10.3390/ijms17121974.

[25] N. Siddiqui, S. Asawa, B. Birru, R. Baadhe, S. Rao, Pcl-based composite scaffold matrices for tissue engineering applications, Mol. Biotechnol. 60 (7) (2018) 506–532, https://doi.org/10.1007/s12033-018-0084-5.

[26] B.D. Ulery, L.S. Nair, C.T. Laurencin, Biomedical applications of biodegradable polymers, J. Polym. Sci. B Polym. Phys. 49 (12) (2011) 832–864, https://doi.org/10.1002/polb.22259.

[27] R. Shi, J. Xue, M. He, D. Chen, L. Zhang, W. Tian, Structure, physical properties, biocompatibility and in vitro/vivo degradation behavior of anti-infective polycaprolactone-based electrospun membranes for guided tissue/bone regeneration, Polym. Degrad. Stabil. 109 (2014) 293–306, https://doi.org/10.1016/j.polymdegradstab.2014.07.017.

[28] N.C.-N. Huynh, V. Everts, A. Nifuji, P. Pavasant, R.S. Ampornaramveth, Histone deacetylase inhibition enhances in-vivo bone regeneration induced by human periodontal ligament cells, Bone 95 (2017) 76–84, https://doi.org/10.1016/j.bone.2016.11.017.

[29] L. Elomaa, S. Teixeira, R. Hakala, H. Korhonen, D.W. Grijpma, J.V. Seppälä, Preparation of poly(ε-caprolactone)-based tissue engineering scaffolds by stereolithography, Acta Biomater. 7 (11) (2011) 3850–3856, https://doi.org/10.1016/j.actbio.2011.06.039.

[30] L. Elomaa, E. Keshi, I.M. Sauer, M. Weinhart, Development of gelma/pcl and decm/pcl resins for 3d printing of acellular in vitro tissue scaffolds by stereolithography, Mater Sci Eng C Mater Biol Appl 112 (2020) 110958, https://doi.org/10.1016/j.msec.2020.110958.

[31] D. Xia, F. Yang, Y. Zheng, Y. Liu, Y. Zhou, Research status of biodegradable metals designed for oral and maxillofacial applications: a review, Bioactive Materials 6 (11) (2021) 4186–4208, https://doi.org/10.1016/j.bioactmat.2021.01.011.

[32] M. Zhao, G. Liu, Y. Li, X. Yu, S. Yuan, Z. Nie, J. Wang, J. Han, C. Tan, C. Guo, Degradation behavior, transport mechanism and osteogenic activity of mg–zn–re alloy membranes in critical-sized rat calvarial defects, Coatings 10 (5) (2020) 496.

[33] Y. Guo, Y. Yu, L. Han, S. Ma, J. Zhao, H. Chen, Z. Yang, F. Zhang, Y. Xia, Y. Zhou, Biocompatibility and osteogenic activity of guided bone regeneration membrane based on chitosan-coated magnesium alloy, Mater. Sci. Eng. C 100 (2019) 226–235, https://doi.org/10.1016/j.msec.2019.03.006.

[34] S. Wu, Y.S. Jang, Y.K. Kim, S.Y. Kim, S.O. Ko, M.H. Lee, Surface modification of pure magnesium mesh for guided bone regeneration: in vivo evaluation of rat calvarial defect, Materials 12 (17) (2019) 2684, https://doi.org/10.3390/ma12172684.

[35] A. Brown, S. Zaky, H. Ray, C. Sfeir, Porous magnesium/plga composite scaffolds for enhanced bone regeneration following tooth extraction, Acta Biomater. 11 (2015) 543–553, https://doi.org/10.1016/j.actbio.2014.09.008.

[36] H. Guo, D. Xia, Y. Zheng, Y. Zhu, Y. Liu, Y. Zhou, A pure zinc membrane with degradability and osteogenesis promotion for guided bone regeneration: in vitro and in vivo studies, Acta Biomater. 106 (2020) 396–409, https://doi.org/10.1016/j.actbio.2020.02.024.

[37] H. Li, T. Qiao, P. Song, H. Guo, X. Song, B. Zhang, X. Chen, Star-shaped pcl/plla blended fiber membrane via electrospinning, J. Biomater. Sci. Polym. Ed. 26 (7) (2015) 420–432, https://doi.org/10.1080/09205063.2015.1015865.

[38] M. Degidi, A. Scarano, A. Piattelli, Regeneration of the alveolar crest using titanium micromesh with autologous bone and a resorbable membrane, J. Oral Implantol. 29 (2) (2003) 86–90.

[39] Y. Wang, M. Ma, J. Wang, W. Zhang, W. Lu, Y. Gao, B. Zhang, Y. Guo, Development of a photo-crosslinking, biodegradable gelma/pegda hydrogel for guided bone regeneration materials, Materials 11 (8) (2018) 1345, https://doi.org/10.3390/ma11081345.

[40] B. Li, Y. Chen, J. He, J. Zhang, S. Wang, W. Xiao, Z. Liu, X. Liao, Biomimetic membranes of methacrylated gelatin/nanohydroxyapatite/poly(l-lactic acid) for enhanced bone regeneration, ACS Biomater. Sci. Eng. 6 (12) (2020) 6737–6747, https://doi.org/10.1021/acsbiomaterials.0c00972.

[41] L. Bai, P. Ji, X. Li, H. Gao, L. Li, C. Wang, Mechanical characterization of 3d-printed individualized ti-mesh (membrane) for alveolar bone defects, J Healthc Eng 2019 (2019) 4231872, https://doi.org/10.1155/2019/4231872.

[42] S. Jin, F. Sun, Q. Zou, J. Huang, Y. Zuo, Y. Li, S. Wang, L. Cheng, Y. Man, F. Yang, J. Li, Fish collagen and hydroxyapatite reinforced poly(lactide- co-glycolide) fibrous membrane for guided bone regeneration, Biomacromolecules 20 (5) (2019) 2058–2067, https://doi.org/10.1021/acs.biomac.9b00267.

[43] V. Cirillo, B.A. Clements, V. Guarino, J. Bushman, J. Kohn, L. Ambrosio, A comparison of the performance of mono- and bi-component electrospun conduits in a rat sciatic model, Biomaterials 35 (32) (2014) 8970–8982, https://doi.org/10.1016/j.biomaterials.2014.07.010.

[44] Q. Wang, Q. Ye, Z. Ma, W. Xie, L. Zhong, Y. Wang, Q. Rong, 3d printed pcl/β-tcp cross-scale scaffold with high-precision fiber for providing cell growth and forming bones in the pores, Mater Sci Eng C Mater Biol Appl 127 (2021) 112197, https://doi.org/10.1016/j.msec.2021.112197.

[45] J. Behring, R. Junker, X.F. Walboomers, B. Chessnut, J.A. Jansen, Toward guided tissue and bone regeneration: morphology, attachment, proliferation, and migration of cells cultured on collagen barrier membranes, A systematic review, Odontology 96 (1) (2008) 1–11, https://doi.org/10.1007/s10266-008-0087-y.

[46] S.M. Meloni, S.A. Jovanovic, I. Urban, E. Baldoni, M. Pisano, M. Tallarico, Horizontal ridge augmentation using gbr with a native collagen membrane and 1:1 ratio of particulate xenograft and autologous bone: a 3-year after final loading prospective clinical study, Clin. Implant Dent. Relat. Res. 21 (4) (2019) 669–677, https://doi.org/10.1111/cid.12808.

[47] Q. Yu, C. Wang, J. Yang, C. Guo, S. Zhang, Mineralized collagen/mg–ca alloy combined scaffolds with improved biocompatibility for enhanced bone response following tooth extraction, Biomed. Mater. 13 (6) (2018), https://doi.org/10.1088/1748-605x/aadb47, 065008.

[48] J. Song, J. She, D. Chen, F. Pan, Latest research advances on magnesium and magnesium alloys worldwide, Journal of Magnesium and Alloys 8 (1) (2020) 1–41, https://doi.org/10.1016/j.jma.2020.02.003.

[49] T. Ahmadi, A. Monshi, V. Mortazavi, M.H. Fathi, S. Sharifi, M. Kharaziha, L. Khazdooz, A. Zarei, M. Taghian Dehaghani, Fabrication and characterization of polycaprolactone fumarate/gelatin-based nanocomposite incorporated with silicon and magnesium co-doped fluorapatite nanoparticles using electrospinning method, Mater Sci Eng C Mater Biol Appl 106 (2020) 110172.

[50] J.W. Lee, H.S. Han, K.J. Han, J. Park, H. Jeon, M.R. Ok, H.K. Seok, J.P. Ahn, K.E. Lee, D.H. Lee, S.J. Yang, S.Y. Cho, P.R. Cha, H. Kwon, T.H. Nam, J.H.L. Han, H.J. Rho, K.S. Lee, Y.C. Kim, D. Mantovani, Long-term clinical study and multiscale analysis of in vivo biodegradation mechanism of mg alloy, Proc. Natl. Acad. Sci. U.S. A. 113 (3) (2016) 716–721, https://doi.org/10.1073/pnas.1518238113.

[51] C.C. Hung, A. Chaya, K. Liu, K. Verdelis, C. Sfeir, The role of magnesium ions in bone regeneration involves the canonical wnt signaling pathway, Acta Biomater. 98 (2019) 246–255, https://doi.org/10.1016/j.actbio.2019.06.001.

[52] H. Zhou, B. Liang, H. Jiang, Z. Deng, K. Yu, Magnesium-based biomaterials as emerging agents for bone repair and regeneration: from mechanism to application, Journal of Magnesium and Alloys 9 (3) (2021) 779–804, https://doi.org/10.1016/j.jma.2021.03.004.

[53] Y. Zhang, J. Xu, Y.C. Ruan, M.K. Yu, M. O'Laughlin, H. Wise, D. Chen, L. Tian, D. Shi, J. Wang, S. Chen, J.Q. Feng, D.H.K. Chow, X. Xie, L. Zheng, L. Huang, S. Huang, K. Leung, N. Lu, L. Zhao, H. Li, D. Zhao, X. Guo, K. Chan, F. Witte, H.C. Chan, Y. Zheng, L. Qin, Implant-derived magnesium induces local neuronal production of cgrp to improve bone-fracture healing in rats, Nat. Med. 22 (10) (2016) 1160–1169, https://doi.org/10.1038/nm.4162.

[54] Y. Zheng, X. Gu, F. Witte, Biodegradable metals, Mater. Sci. Eng. R Rep. 77 (2014) 1–34, https://doi.org/10.3390/books978-3-03897-387-4.

[55] L.Y. Li, L.Y. Cui, R.C. Zeng, S.Q. Li, X.B. Chen, Y. Zheng, M.B. Kannan, Advances in functionalized polymer coatings on biodegradable magnesium alloys - a review, Acta Biomater. 79 (2018) 23–36, https://doi.org/10.1016/j.actbio.2018.08.030.

[56] Y. Chen, Y. Song, S. Zhang, J. Li, C. Zhao, X. Zhang, Interaction between a high purity magnesium surface and pcl and pla coatings during dynamic degradation, Biomed. Mater. 6 (2) (2011), https://doi.org/10.1088/1748 6041/6/2/025005, 025005.